Practical 15 Mb/s Quantum Key Distribution Using Compact Single-Photon Detectors

Tingting Shi(施婷婷)[1†], Zhengyu Yan(阎正宇)[1†], Yuanbin Fan(范元滨)[1*], Lai Zhou(周来)[1], Yuanfei Gao(高远飞)[1], Davide G. Marangon[2], and Zhiliang Yuan(袁之良)[1]

[1]*Beijing Academy of Quantum Information Sciences, Beijing 100193, China*
[2]*Department of Engineering of Information, Padua University, Italy*

(Received 9 September 2025; accepted manuscript online 5 November 2025)

Quantum key distribution (QKD) is recognized as an unconditionally secure method of communication encryption, relying solely on the principles of quantum mechanics. A key performance metric for QKD systems is secure key rate (SKR), which is a critical factor for real-world applications. Herein, we report a practical QKD system, equipped with compact gated InGaAs/InP single-photon detectors (SPDs), that can generate a high SKR of 15.2 Mb/s with a channel loss of 2 dB. This exceptional performance stems from the ultra-low afterpulsing probability of the SPDs, which significantly reduces the bit error rate in the QKD system. The typical quantum bit error rate is 1.3%. The results validate the feasibility of an integrated, practical QKD system and offer a reliable solution for the future development of real-world QKD networks.

DOI: 10.1088/0256-307X/42/12/120602 CSTR: 32039.14.0256-307X.42.12.120602

1. Introduction. Information-theoretically secure communication delivers the ultimate level of assurance. Quantum Key Distribution (QKD) makes this possible by allowing two remote parties to produce and distribute a random, secure key that can be used in symmetric cryptography protocols, such as the one-time pad for perfect secrecy. First proposed 40 years ago,[1,2] QKD has seen significant technological progress over the past decade, finally being used in practical, real-world applications. In fact, QKD can be used to support secure network services in various fields. It protects the transmission of financial data, such as banking transactions, and secures medical data storage for patient privacy. QKD also safeguards critical infrastructure, such as power grids and transportation systems, as well as mobile internet communications.[3–5]

For all these applications, the most important figure of merit is the secret key rate (SKR), that is, the rate at which the encryption keys are generated. A higher SKR enables QKD networks to update secret keys more frequently, thereby strengthening communication security. This practical aspect has prompted the exploration of different approaches to increase it. The primary approach is to boost the clock rate on the transmitter side and increase the number of qubits transmitted per unit time. Another approach focuses on optimizing the receiver side, where most QKD systems now employ compact InGaAs/InP single-photon detectors (SPDs) operated in gated-mode devices that have undergone significant improvements in recent years.[6–8] Reducing dark counts and afterpulses, the two primary noise sources, lowers the qubit error rate (QBER) while enhancing the detection efficiency minimizes the loss of qubits.[9] Optimizing both the transmitter and receiver enables QKD systems to achieve exceptionally high SKR. For instance, the system reported by Yuan *et al.*[10] operates at gigahertz clock rate, delivering a real-time SKR of 13.72 Mb/s over a 2 dB channel (equivalent to 10 km optical fiber) using InGaAs/InP SPDs.

Herein, we report a practical QKD system incorporating recent advancements in both transmitter and receiver designs. The system employs a time-bin-encoded decoy-BB84 protocol[11,12] operating at a 1.25 GHz clock rate. The transmitter uses a recently developed in-phase/quadrature (IQ) modulator to suppress the code patterning effect.[13] The receiver leverages advanced InGaAs/InP SPDs,[6–8] which are capable of sustaining count rates of up to 200 Mcps while maintaining a very low afterpulsing probability. With these optimizations, we achieved a record SKR of 15.2 Mb/s with a channel loss of 2 dB for an InGaAs-SPD-based QKD system.

2. Protocol. The most practical QKD protocol in use today combines the standard BB84 scheme with the decoy-state method,[11,12] which has been proven secure against general attacks even in the finite-key regime.[14–16] In this protocol, the transmitter (Alice) encodes quantum information onto weak coherent pulses (WCPs) emitted by a laser source. As a WCP follows a Poisson-like photon number distribution, some pulses inevitably contain more than one photon. An eavesdropper (Eve) could, in principle, exploit these multi-photon pulses by performing a photon-number-splitting attack.[17] The decoy-state technique addresses this vulnerability by randomly varying the mean photon number of the transmitted pulses among different

†These authors contributed equally to this work.
*Corresponding author. Email: fanyb@baqis.ac.cn
© 2025 Chinese Physical Society and IOP Publishing Ltd. All rights, including for text and data mining, AI training, and similar technologies, are reserved.

intensity levels, including a signal state and one or more decoy states. By comparing the detection probabilities and error rates corresponding to these different intensities, Alice and Bob can conservatively estimate the contribution of single-photon pulses and then tightly bound Eve's information. This allows them to distill a secure key, even in the presence of multi-photon components and channel loss. Consequently, decoy-state BB84 allows high key rates and long-distance secure transmission with practical laser sources.

In 2020, Yin *et al.* introduced a rigorous and optimal analytical formula to address statistical fluctuations, thereby ensuring security against general attacks in the finite-key regime.[16] The SKR derived by Yin *et al.* is expressed by the following equation:

$$R = \underline{s}_0^Z + \underline{s}_1^Z\left[1 - \mathrm{h}\left(\overline{\phi}_1^Z\right)\right] - \lambda_{\mathrm{EC}} - \log_2\frac{2}{\varepsilon_{\mathrm{cor}}} - 6\log_2\frac{23}{\varepsilon_{\mathrm{sec}}}, \tag{1}$$

where $\underline{s}_0^Z$, $\underline{s}_1^Z$, and $\overline{\phi}_1^Z$ represent the lower bounds for the number of vacuum events, single-photon events, and the upper bound for the phase error rate associated with single-photon events in the raw key reconciliation basis Z, respectively. The term $\mathrm{h}(x) = -x\log_2 x - (1-x)\log_2(1-x)$ is the binary Shannon entropy function, and λ_{EC} accounts for error correction leakage. $\varepsilon_{\mathrm{cor}}$ and $\varepsilon_{\mathrm{sec}}$ are security parameters satisfying $\varepsilon_{\mathrm{cor}} + \varepsilon_{\mathrm{sec}} \leq \varepsilon$ (error rate), which guarantees protocol security. Since the introduction of near-optimal analytical formulas to address statistical fluctuations, this method has achieved a higher SKR and extended the secure transmission distance beyond that offered by other approaches.

3. Experiment. Our QKD system's design is illustrated in Fig. 1(a). At the transmitter (Alice), a BB84 protocol is implemented using a 1550 nm gain-switched DFB laser diode, which generates 30 ps optical pulses at a 1.25 GHz repetition rate. An IQ modulator encodes pulse intensities for the decoy protocol [Fig. 1(b)], as detailed in Section 3.1, and an asymmetric Mach-Zehnder interferometer (AMZI) with phase modulators (PMs) encodes qubit phases. Then, a variable optical attenuator attenuates the light to the desired single-photon levels requested by the protocol. At the receiver side (Bob), the qubit decoder employs another AMZI with two PMs. The encoding and decoding modules are described further in Section 3.2. Two compact SPD modules [Fig. 1(c)], gated at 1.25 GHz, follow the AMZI; their advanced features ensure a very low QBER, as discussed in Section 3.3.

3.1. Decoy-State Generation. In the decoy-state BB84 protocol, the transmitter randomly adjusts pulse intensities to ensure security against photon-number-splitting attacks.[17] These intensity levels of the signal (S), decoy (D), and vacuum (V) are generated using intensity modulators driven by fast digital-to-analog converters. However, decoy levels often exhibit a patterning effect in which the pulse intensities are biased depending on the preceding transitions, as detailed in several works.[13,18–20] This poses a clear side-channel risk because correlated intensity levels could enable an eavesdropper to exploit these patterns, a challenge that our system bypasses by adopting another method to implement the decoy levels.

Our QKD system utilizes an IQ modulator to prepare the three intensity states. The IQ modulator consists of two parallel Mach-Zehnder interferometers (MZIs): the in-phase component (I-MZI) and quadrature component (Q-MZI), as shown in Fig. 1(b). The RF voltages V_{RFI} and V_{RFQ} are set to the half-wave switching voltage V_π, whereas the DC bias voltages V_{BI}, V_{BQ}, and $V_{\mathrm{BG}\pm}$ are

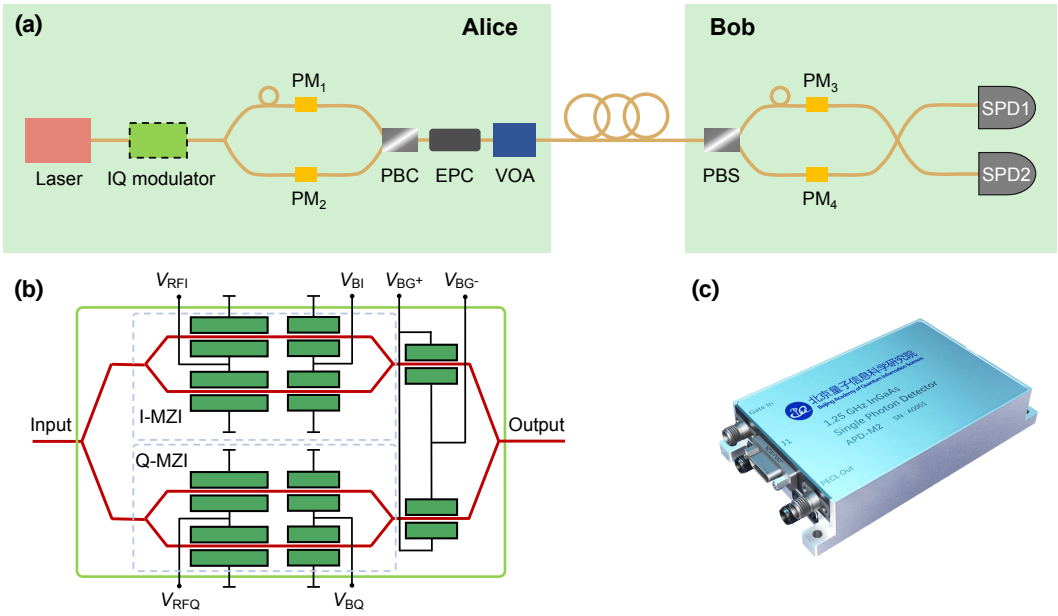

Fig. 1. (a) Schematic of QKD system-based decoy-state BB84 protocol. IQ modulator: in-phase/quadrature (IQ) modulator, PM: phase modulator, PBC: polarization beam combiner, EPC: electronic polarization controller, VOA: variable optical attenuator, PBS: polarization beam splitter, SPD: single-photon detector. (b) Schematic of the IQ modulator. (c) Photo of a UNIC-SPD module.

adjustable to induce phase shifts in the sub-DC ports I-MZI and Q-MZI and the primary DC port IQ-MZI, respectively. By fine-tuning these three DC voltages, the IQ modulator can generate three distinct intensities with ratios $[s : d : v]$. The extinction ratio $[s : v]$ can reach 30 dB.

To select the optimal intensity ratios, we followed [16] and assumed a block size of 10^8. Figure 2 shows the simulation [16] of the SKR as a function of signal and decoy photon flux for transmission over 10 km of fiber, using parameters consistent with the experimental data. The optimal intensity ratio of signal to decoy states was found to be $[s : d] = [1 : 0.5]$; similarly, the optimal generation probabilities for the three states were found to be $[p_s : p_d : p_v] = [64\% : 32\% : 4\%]$. Figure 2 demonstrates that with these optimal choices, the simulations predict that the maximum SKR can exceed 15 Mbit/s.

The intensity output of the IQ modulator can be expressed as

$$I_{\text{out}} = |E|^2 = \frac{I_{\text{in}}}{16}\Big|(\mathrm{e}^{-j\frac{\theta_{\text{I}}}{2}} + \mathrm{e}^{j\frac{\theta_{\text{I}}}{2}})\mathrm{e}^{-j\frac{\theta_{\text{G}}}{2}} + (\mathrm{e}^{-j\frac{\theta_{\text{Q}}}{2}} + \mathrm{e}^{j\frac{\theta_{\text{Q}}}{2}})\mathrm{e}^{j\frac{\theta_{\text{G}}}{2}}\Big|^2, \quad (2)$$

where θ_{I}, θ_{Q}, and θ_{G} are the different phases of the I-MZI, Q-MZI, and IQ-MZI, respectively. In practice, to satisfy $[s : d] = [1 : 0.5]$, θ_{G} is set to $\pi/2$ by adjusting the DC V_{BG}. The IQ output intensity as a function of θ_{I} and θ_{Q} is shown in Fig. 3(a). The peak point S ($\theta_{\text{I}} = \theta_{\text{Q}} = 0$) is used to generate the signal state, and the valley point V ($\theta_{\text{I}} = \theta_{\text{Q}} = \pi$) is used to generate the vacuum state. The saddle points D_1 ($\theta_{\text{I}} = \pi$, $\theta_{\text{Q}} = 0$) and D_2 ($\theta_{\text{I}} = 0$, $\theta_{\text{Q}} = \pi$) correspond to the decoy states. The partial derivatives of these states are all zero, ensuring maximal suppression of pattern effects. However, the two sub-MZIs are not perfectly identical; thus, two decoy states of different intensities are observed in the output. [13] Consequently, one decoy state must be fixed. To verify the absence of the patterning effect, we measured the output of the IQ modulator using a fast photodiode and digital oscilloscope. Figure 3(b) shows the oscilloscope traces for the intensities of the S and D pulses with three types of predecessors: the s, d, and v states. One can appreciate the effectiveness of the IQ modulator in mitigating the patterning effect. Indeed, the amplitudes of the decoy and signal pulses are nearly identical, regardless of their predecessors.

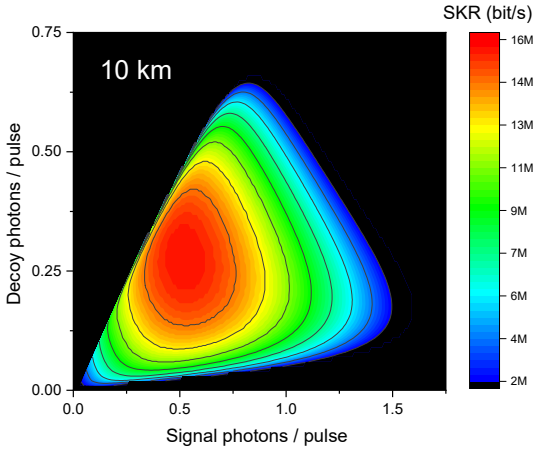

Fig. 2. Simulation of SKR as a function of signal and decoy photon flux over 10 km of fiber. The preferred intensity ratio of decoy to signal states is 0.5, and the maximum SKR can reach over 15 Mbit/s.

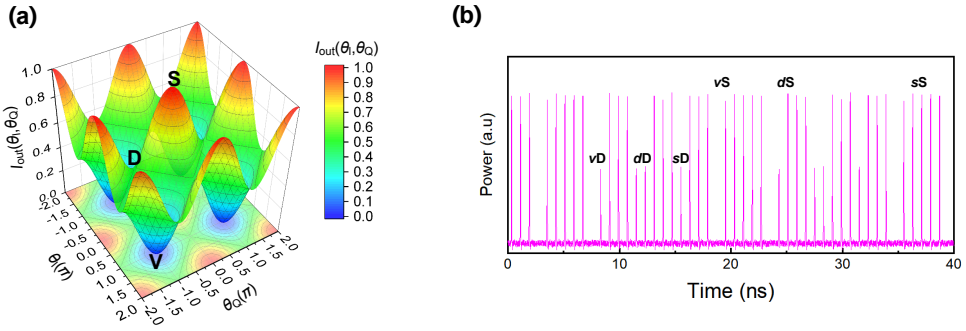

Fig. 3. (a) Simulation of the IQ output intensity as a function of θ_{I} and θ_{Q}. The peak point S ($\theta_{\text{I}} = \theta_{\text{Q}} = 0$) is used to generate the signal state, and the valley point V ($\theta_{\text{I}} = \theta_{\text{Q}} = \pi$) is used to generate the vacuum state. The saddle points D_1 ($\theta_{\text{I}} = \pi, \theta_{\text{Q}} = 0$) and D_2 ($\theta_{\text{I}} = 0$, $\theta_{\text{Q}} = \pi$) correspond to the decoy states. (b) Oscilloscope traces for IQ modulators, including patterns sS, dS, vS, sD, dD, vD.

3.2. Phase Encoding System. The information is encoded and decoded in the phase of a photon using a pair of AMZIs based on the BB84 protocol. [1,21] The transmitter (Alice) and receiver (Bob) each use an AMZI with a differential delay of approximately 400 ps, corresponding to half the transmission repetition period (800 ps). By setting the driving voltages of the electric polarization controller (EPC) optimally, each photon will be routed through either the short arm of one AMZI and the long arm of the other, or vice versa. Interference occurs at Bob's exit beam splitter between these two indistinguishable paths. When polarization drifts from the optimal state, the count rate of the SPDs will decrease. By promptly adjusting the voltage applied to the EPC, the polarization state can be effectively controlled and stabilized. The phase difference between the two paths is controlled by four PMs, which determine the interference conditions. PM1 randomly prepares one of the two phases $\phi_1 = \{0, \pi\}$ for the key states $|0\rangle$ and $|1\rangle$. PM2 and PM3 prepares one of the two phases ϕ_2 and $\phi_3 = \{0, \pi/2\}$ for the bases X and Z, respectively.

Table 1. List of parameter settings. f is system clock frequency; s, d, v and P_s, P_d, P_v are the mean photon numbers and probabilities for signal, decoy, and vacuum states, respectively; P_Z, P_X are the probabilities of Alice and Bob choosing the Z, X basis, respectively; f_{EC} is error correction coefficiency.

Parameter	Setting
f	1.25 GHz
s, d, v	1: 0.5: 0.003
P_s, P_d, P_v	64%, 32%, 4%
P_Z, P_X	94%, 6%
Datasize	100 Mb
Bob's loss	2.7 dB
Detection efficiency	26%(SPD1), 27%(SPD2)
Afterpulsing probability	0.5%(SPD1), 0.9%(SPD2)
Dark count probability	1.36×10^{-5} gate^{-1}(SPD1), 1.52×10^{-5} gate^{-1}(SPD2)
f_{EC}@QBER=1.3%	1.05

By analyzing the real-time variations of the QBER, PM4 can be used to compensate for additional phase differences caused by real-time temperature and vibration fluctuations, thereby maintaining the QBER at a minimal level. Owing to polarization matching and the nearly identical optical path lengths in the long arms, the interference visibility of this AMZI pair exceeds 99.2%.

In the present QKD system, the Z basis is encoded with a probability of $P_Z = 94\%$ for key distillation, whereas the X basis has a 6% probability of assessing information leakage. This asymmetric allocation between encoding bases enhances the key generation efficiency [22] and minimizes the fraction of data ($2P_XP_Z$) originating from mismatched bases that must be discarded. Considering a signal state transmission probability of $P_s = 0.64$, the total sifting efficiency is 0.57, as obtained from $\eta_{\mathrm{sift}} = P_sP_Z^2$. The specific parameter settings are summarized in Table 1, aiming at a high SKR over a short fiber distance of 10 km.

3.3. Compact Single-Photon Detector Module. Photon detection is conducted using two compact SPD modules. [7] Each module measures just $8.8\times6\times2\,\mathrm{cm}^3$, as shown in Fig. 1(c). The form factors of these detectors make them suitable for building compact QKD receiver units that can be easily fitted into standard 19-inch rack mounts. The afterpulse probability of the detector represents a significant limiting factor in achieving a high SKR. To address this, we use our previously reported ultra-narrowband interference circuits (UNICs) to mitigate the strong capacitive response during sub-nanosecond gating, effectively suppressing afterpulsing. [6,7] The UNICs integrate a surface acoustic wave (SAW) filter into an asymmetric radio-frequency Mach–Zehnder interferometer. The long group delay of the SAW filter enables the UNIC interferometer to achieve ultra-narrowband rejection, with manufacturing tolerances easily satisfied within the RF track lengths. Consequently, UNICs provide a wide and continuous passband in the frequency domain, which minimizes distortion of the avalanche signal while suppressing afterpulsing. The compact SPD modules used in the QKD system not only incorporate readout circuits but also include regulation and compensation mechanisms to account for temperature drift and temperature-dependent group delay of the SAW filter. Owing to the well-designed circuits, these detectors can operate stably under varying ambient conditions, making them suitable for practical applications.

An inherent trade-off is observed between detector afterpulsing and dark count rate when optimizing system performance. Operating the detector at a lower temperature reduces the dark count probability but worsens the afterpulsing behavior. However, for short fiber links, dark counts contribute minimally to the QBER, with afterpulsing being the dominant source of errors. Because our system is designed to achieve high SKRs over short distances, we prioritize the optimization of the afterpulsing characteristics, which leads to a higher dark count rate; nevertheless, this has a negligible effect on the overall QBER. In this study, Bob's SPDs were gated at a frequency of 1.25 GHz, and we adjusted the operating temperature of the APD to 30 ℃ to achieve low afterpulsing probabilities of 0.5% and 0.9% corresponding to detection efficiencies of 26% and 27%, respectively, under a 3 ns hold-off time, with dark count rates of 1.36×10^{-5}/gate and 1.52×10^{-5}/gate, respectively.

4. Results and Discussion. Our QKD system implements the decoy-state QKD protocol, and we chose a dataset size of 10^8 to mitigate finite-size effects caused by statistical fluctuations. Figure 4(a) shows the raw bit rate, SKR, and QBER for different signal photon fluxes obtained by varying the VOA in a 2 dB attenuation channel. The optimal signal state intensity is approximately 0.5, enabling a maximum SKR (red) of 15.2 Mb/s. The SPDs have a maximum count rate of 220 MHz, constraining the raw bit rate (black) to approximately 80 Mbit/s. The system achieves a low typical QBER (yellow) of 1.2%. Figure 4(b) shows SKR as a function of QBER for the same loss of 2 dB. As anticipated, these performances are primarily due to our SPD modules, which feature ultralow afterpulsing probability and high detection efficiency.

To assess system stability in a scenario that approximates real-world conditions, we conducted experiments using a 10 km standard single-mode fiber with a channel loss of 2 dB, which realistically reflects photon polarization drift and fluctuations. EPC was employed to correct for polarization drift in real time, thereby optimizing the efficiency of the interferometer. In the 10 km optical fiber experiment, the raw bit rate, SKR, and QBER as functions of signal photon flux are shown in Fig. 4(c). The maximum SKR (red) reaches close to 14.2 Mb/s, with a corresponding QBER (yellow) of 1.3%. These results are in good agreement with the simulated data. Notably, our QKD system surpasses the previous record of 13.72 Mbit/s for systems implemented with practical InGaAs SPDs. [10] Table 1 details our parameter settings. Note that Bob's loss of 2.7 dB in the present system is 0.7 dB higher than that of the previous state-of-the-art system. [10] Nevertheless, the enhanced clock rate and optimized afterpulsing performance enable our system to surpass the previous SKR record.

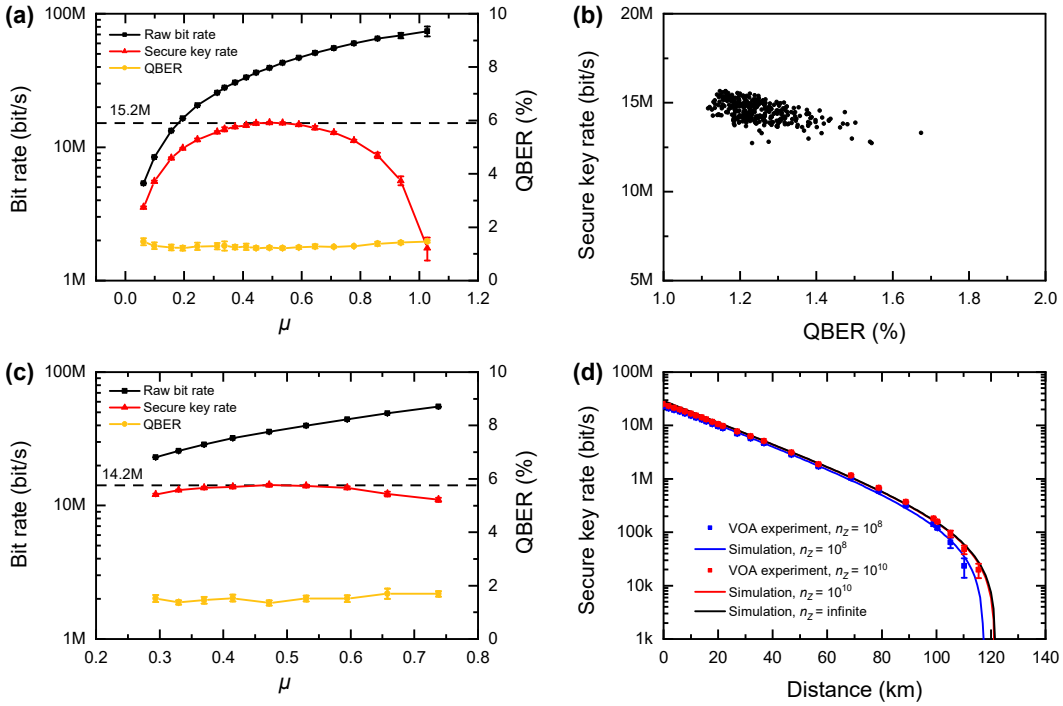

Fig. 4. (a) Raw bit rate, SKR, and QBER as functions of signal photon flux in a 2 dB attenuation channel, varied by adjusting the attenuation of the VOA. The preferred intensity of signal states is approximately 0.53, and the maximum SKR can reach 15.2 Mbit/s. (b) SKR as a function of QBER in a 2 dB attenuation channel. (c) Raw bit rate, SKR, and QBER as functions of signal photon flux in the 10-km optical fiber. (d) SKRs at different fiber distances for finite block sizes of $n_Z = 10^8$ and $n_Z = 10^{10}$.

To evaluate the dependence of SKR on the transmission distance, we conducted a series of experiments by adjusting the VOA attenuation to simulate varying optical fiber lengths. Experimental data and theoretical simulations are represented by points and solid lines in Fig. 4(d), respectively. Here, we use two different data block sizes: 10^8 and 10^{10}. With either block size setting, the SKRs closely align with the simulated values. The maximum secure transmission distance is 120 km. The blue line indicates that the QKD system can secure a transmission distance of up to 115 km using the BB84 protocol with the decoy state method for a finite block size of $n_Z = 10^8$. When the finite block size increases 10^{10}, the results closely approach the infinite key scenario.

5. Conclusion. We reported a QKD system featuring compact InGaAs/InP SPDs that achieves an SKR of 15.2 Mb/s with channel losses of 2 dB and 10 Mb/s over 20 km of ultralow-loss fiber (3.2 dB loss). This exceptional performance is primarily attributed to the ultralow afterpulsing probability, high detection efficiency, and low-error codecs of our compact SPDs. The system maintains a low typical QBER of 1.3%. In the future, we anticipate that our UNIC detector technology can be further developed to support multi-gigahertz operation, similar to those using alternative circuits,[23–26] thus enabling substantially higher SKRs. In combination with the wavelength-division multiplexing of multiple quantum channels, this strategy offers a clear route toward high-speed QKD with SKRs beyond 100 Mb/s, a rate that has recently been demonstrated with SNSPD single-photon detectors[9] requiring cryogenic cooling.

Acknowledgements. This work was supported by the Innovation Program for Quantum Science and Technology (Grant No. 2024ZD0302500), the National Natural Science Foundation of China (Grant No. 62250710162), and the Beijing Natural Science Foundation (Grant No. Z230005).

References

[1] Bennett C H and Brassard G 2014 *Theor. Comput. Sci.* **560** 7
[2] Ekert A K 1991 *Phys. Rev. Lett.* **67** 661
[3] Diamanti E, Lo H K, Qi B, and Yuan Z 2016 *npj Quantum Inf.* **2** 16025
[4] Xu F, Ma X, Zhang Q, Lo H K, and Pan J W 2020 *Rev. Mod. Phys.* **92** 025002
[5] Mehic M, Niemiec M, Rass S, Ma J J, Peev M, Aguado A, Martin V, Schauer S, Poppe A, Pacher C, and Voznak M 2020 *ACM Comput. Surv.* **53** 1
[6] Fan Y B, Shi T T, Ji W J, Zhou L, Ji Y, and Yuan Z L 2023 *Opt. Express* **31** 7515
[7] Yan Z Y, Shi T T, Fan Y B, Zhou L, and Yuan Z L 2023 *Adv. Devices & Instrum.* **4** 0029
[8] Shi T T, Fan Y B, Yan Z Y, Zhou L, Ji Y, and Yuan Z L 2024 *J Semicond.* **45** 032702
[9] Li W, Zhang L K, Tan H, Lu Y C, Liao S K, Huang J, Li H, Wang Z, Mao H K, Yan B Z, Li Q, Liu Y, Zhang Q, Peng C Z, You L X, Xu F H, and Pan J W 2023 *Nat. Photonics* **17** 416
[10] Yuan Z L, Plews A, Takahashi R, Doi K, Tam W, Sharpe A W, Dixon A R, Lavelle E, Dynes J F, Murakami A, Kujiraoka M, Lucamarini M, Tanizawa Y, Sato H, and Shields A J 2018 *J. Lightwave Technol.* **36** 3427
[11] Wang X B 2005 *Phys. Rev. Lett.* **94** 230503

[12] Lo H K, Ma X, and Chen K 2005 *Phys. Rev. Lett.* **94** 230504
[13] Gao Y F and Yuan Z L 2023 *Opt. Lett.* **48** 1068
[14] Lim C C W, Curty M, Walenta N, Xu F H, and Zbinden H 2014 *Phys. Rev. A* **89** 022307
[15] Rusca D, Boaron A, Grünenfelder F, Martin A, and Zbinden H 2018 *Appl. Phys. Lett.* **112** 171104
[16] Yin H L, Zhou M G, Gu J, Xie Y M, Lu Y S, and Chen Z B 2020 *Sci. Rep.* **10** 14312
[17] Brassard G, Lütkenhaus N, Mor T, and Sanders B C 2000 *Phys. Rev. Lett.* **85** 1330
[18] Yoshino K I, Fujiwara M, Nakata K, Sumiya T, Sasaki T, Takeoka M, Sasaki M, Tajima A, Koashi M, and Tomita A 2018 *npj Quantum Inf.* **4** 8
[19] Roberts G, Pittaluga M, Minder M, Lucamarini M, Dynes J, Yuan Z, and Shields A 2018 *Opt. Lett.* **43** 5110
[20] Lu F Y, Lin X, Wang S, Fan-Yuan G J, Ye P, Wang R, Yin Z Q, He D Y, Chen W, Guo G C, and Han Z F 2021 *npj Quantum Inform.* **7** 75
[21] Bennett C H 1992 *Phys. Rev. Lett.* **68** 3121
[22] Lucamarini M, Patel K, Dynes J, Fröhlich B, Sharpe A, Dixon A, Yuan Z, Penty R, and Shields A J 2013 *Opt. Express* **21** 24550
[23] He D Y, Wang S, Chen J L, Chen W, Yin Z Q, Fan-Yuan G J, Zhou Z, Guo G C, and Han Z F 2023 *Adv. Devices & Instrum.* **4** 0020
[24] Yuan Z L, Sharpe A, Dynes J, Dixon A, and Shields A 2010 *Appl. Phys. Lett.* **96** 071101
[25] Namekata N, Takesue H, Honjo T, Tokura Y, and Inoue S 2011 *Opt. Express* **19** 10632
[26] Zhang J, Eraerds P, Walenta N, Barreiro C, Thew R, and Zbinden H 2010 *Proc. SPIE* **7681** 239